Frequent in-frame somatic deletions activate gp130 in inflammatory hepatocellular tumours

Sandra Rebouissou[1,2], Mohamed Amessou[1,2], Gabrielle Couchy[1,2], Karine Poussin[1,2], Sandrine Imbeaud[3,4], Camilla Pilati[1,2], Tina Izard[5], Charles Balabaud[6,7], Paulette Bioulac-Sage[6,8], Jessica Zucman-Rossi[1,2]**

[1]Inserm, U674, Génomique fonctionnelle des tumeurs solides, Paris, F-75010 France

[2]Université Paris Diderot - Paris 7, Institut Universitaire d'Hématologie; Paris, F-75010 France

[3]Array s/IMAGE, Genexpress, Functional Genomics and Systems Biology for Health, UMR 7091 CNRS; Université Paris 6 Pierre et Marie Curie, Villejuif, F-94801 France

[4]Gif/Orsay DNA Microarray Platform (GODMAP), Centre de Génétique Moléculaire, UPR 2167 CNRS, Gif-sur-Yvette, F-91198 France; Université Paris-Sud 11, Orsay, F-91405 France

[5]Department of Cancer Biology, The Scripps Research Institute, Jupiter, Florida, USA

[6]Inserm, U889; Université Victor Segalen Bordeaux 2, IFR66, Bordeaux, F-33076, France.

[7]CHU de Bordeaux, Hopital Saint-André, Service d'hépatologie, Bordeaux, F-33076, France

[8]CHU de Bordeaux, Hopital Pellegrin, Service d'Anatomie Pathologique, Bordeaux, F-33076, France

**Correspondence to: Jessica Zucman-Rossi, Inserm, U674, CEPH-Fondation Jean Dausset, IUH-Saint-Louis, 27 rue Juliette Dodu, 75010 Paris, France. TEL: 33 1 53 72 51 66. FAX: 33 1 53 72 51 58. Email: zucman@cephb.fr

Short title: gp130 mutations in hepatocellular tumours

List of Key genes/proteins: GP130, IL6ST, IL-6, β-catenin, CTNNB1, HNF1A, IFN, STAT3, SAA, CRP, JAK1, JAK2, STAT1, STAT2, IL11

Inflammatory hepatocellular adenomas (IHCA) are benign liver tumours defined by the presence of inflammatory infiltrates and by the elevated expression of inflammatory proteins in tumour hepatocytes[1,2]. Here we show a striking activation of the IL6 signalling pathway in this tumour type, and sequencing candidate genes pinpointed this response to somatic gain-of-function mutations in the *IL6ST* gene that encodes the signalling co-receptor gp130. Indeed, 60% of IHCA harbour small in-frame deletions that target the binding site of gp130 for IL6, and expression of four different gp130 mutants, in hepatocellular cells, activates STAT3 in absence of ligand. Further, analysis of hepatocellular carcinomas revealed that rare gp130 alterations are always accompanied by β-catenin-activating mutations, suggesting a cooperative effect of these signalling pathways in the malignant conversion of hepatocytes. The recurrent gain-of-function gp130 mutations in these human hepatocellular adenomas fully explains activation of the acute inflammatory phase observed in tumourous hepatocytes, and suggests that similar alterations may occur in other inflammatory epithelial tumours having STAT3 activation.

Several recent studies have shown STAT3 activation in epithelial tumours, underscoring the importance of IL6 signalling and the inflammatory response in tumourigenesis, which provides an opportunity for therapeutic intervention[3]. However, the mechanisms that provoke sustained STAT3 activation in tumours are largely unresolved. To define the interaction between the inflammatory response and carcinogenesis in liver tumours, we assessed inflammatory hepatocellular adenomas (IHCA), benign tumours predominately found in women and frequently associated with obesity and alcohol use[1,2]. Tumour hepatocytes of these adenomas express elevated levels of serum amyloid A (SAA) and C-reactive (CRP) proteins, two

members of the acute-phase inflammatory response, whereas SAA and CRP are not expressed in inflammatory cells, Kupffer cells, or other sinusoidal cells in IHCA (Fig. 1a, Supplementary Fig. S1, and Ref. 1). Inflammatory infiltrates were largely localised to arterial vessels, but were also found within the sinusoidal lumens of IHCA. Here, CD45+CD3+ T lymphocytes (CD4:CD8, 2:1) were intermingled with less numerous CD20+CD79A+ B cells, some plasma cells and a few polymorphonuclear cells; no CD30+ lymphocytes, nor CD56+ or CD57+ NK cells were observed. In addition, CD68+ histiocytes were present in infiltrates, as well as prominent Kupffer cells in sinusoidal lumens (Supplementary Fig. S1). Overall, inflammatory infiltrates observed in IHCA were highly polymorphous.

To resolve the underlying pathogenesis of these inflammatory lesions, a genome-wide transcriptome analysis of four IHCA was compared to four normal liver tissue samples. Among the 285 genes significantly overexpressed in IHCA (Supplementary Table S1), gene ontology analysis identified a strong enrichment for genes associated with inflammation and the immune response, accounting for 40% of the overall terms significantly enriched (Supplementary Table S2). High levels of significance were found for “antigen processing and presentation of peptide antigen” (P=2.10^{-11}) and “regulation of the JAK/STAT cascade” (P=10^{-5}) (Supplementary Table S2). We confirmed this inflammatory signature in an additional 14 IHCA with a clear activation of the acute-phase inflammatory response affecting both type-1 and type-2 acute-phase genes (Fig. 1b and 1c, Supplementary Table S3). Consistent with the known roles of IL6 and JAK-STAT signalling in the acute-phase response[4,5], STAT3 mRNA and protein were significantly elevated in IHCA (Fig. 1b and 1c). IHCA also overexpressed several effectors of type-1 and type-2 interferon signalling pathways (*e.g.*, JAK2, STAT1 and STAT2) and their downstream targets (Fig. 1b,

1c). Collectively, these data suggest that IL6 and interferon signalling are the main inflammatory pathways activated in IHCA (Fig. 1d).

Since IL6 was not overexpressed in IHCA and because the inflammatory response was restricted to tumour hepatocytes (Fig. 1a), we reasoned that somatic genetic mutation(s) might account for activation of IL6 receptor signalling in IHCA. We selected *IL6ST* as a candidate gene since it encoded the cell surface signalling receptor gp130 shared by at least six different cytokines including IL6, IL11, LIF, OSM, CTNF and CT-1[4,6]. We sequenced the entire gp130 coding region in 43 IHCA and 33 non-inflammatory hepatocellular adenomas. Remarkably, 26 mutations in gp130 were identified specifically in 60% (26/43) of IHCA, and these included 16 unique, small in-frame deletions and one 33 bp in-frame duplication in exon 6 (Fig. 2a and Table 1). Notably, all *IL6ST* mutations were found in IHCA and all were of somatic origin, as they were not observed in adjacent normal liver tissues. In all cases, *IL6ST* mutations were monoallelic, and IHCA with these mutations expressed both the wild type and mutated alleles at comparable levels, as judged by sequencing RT-PCR products of *IL6ST* mRNA (Supplementary Fig. S2).

Binding of IL-6 to its cognate receptor gp80 (encoded by *IL6R*) induces formation of a high affinity ternary hexameric complex consisting of two molecules each of IL6, IL6R and gp130[7,8]. Gp130 engagement then activates JAK/Tyk tyrosine kinases and the STAT family of transcription factors[9-11]. The consequences of the *IL6ST* in-frame deletions observed in IHCA included the removal of 1 to 26 amino acids neighbouring the IL6/IL6R binding site (also known as CHR E-F loop) located in D2 domain of gp130 (Fig. 2b). We modelled the different deletions and the duplication in the known crystal structure of the wild type IL6/IL6R/gp130 ternary complex (PDB 1P9M)[7]. All of these mutations are predicted to disrupt key residues

involved in the gp130-IL6 interface. Specifically, the most frequent alterations target residues 186-191, which direct the gp130-IL6 interaction, whereas the remaining deletions and duplication affect the other two loops that contribute to gp130-IL6 interactions (Fig. 2b). Therefore, the gp130-IL6 interface is targeted in IHCA.

To investigate possible functional consequences of these gp130 mutations, we tested the effects of enforced expression of two frequent deletions (S187_Y190del and Y186_Y190del) and two infrequent mutants (V184_Y186del, S187A and K173_D177del) in Hep3B cells, a hepatocellular carcinoma line that activates the acute inflammatory phase following IL6 treatment[12]. In the absence of IL6 ligand and serum, overexpression of wild type gp130 alone was not sufficient to activate STAT3 and the downstream acute-phase inflammatory genes (Fig. 3 and Refs. [7,13]). In contrast, all gp130 IHCA mutants activated an acute phase inflammatory response and induced typical targets of this response, including *CRP*, *SAA2*, *SPINK1* and *FBG* (Fig. 3a, 3c). Further, as observed in IHCA, all of these gp130 mutants induced the expression of *SOCS3*, which normally serves to harness cytokine signalling (Fig. 3a). Mutant gp130 S187_Y190del was constitutively tyrosine phosphorylated and the activity of STAT3 was clearly increased in gp130 S187_Y190del-expressing Hep3B cells (Fig. 3b). Similarly, immunohistochemical analyses of IHCA demonstrated marked increases in nuclear STAT3 phosphorylated at Tyr-705 (Supplementary Fig. S4e-f). Finally, IL6 augmented the induction of *CRP* in gp130 S187_Y190del-expressing cells, but mutant receptors were not hypersensitive to low doses of IL6 (Fig. 3d). Therefore, gp130 mutants are constitutively active, and they activate STAT3 and inflammatory response genes in the absence of IL6.

A critical step in the activation of intracellular signalling after IL6 binding on gp130 is the formation a hexameric structure that juxtaposes the membrane proximal

domains of two gp130 molecules at the cell surface[7,14,15]. Using co-immunoprecipitation, we showed that the gp130 S187_Y190del IHCA mutant was able to homodimerize or heterodimerize with wild-type gp130 independently of IL6, whereas wild-type gp130 cannot homodimerize (Fig. 3f). Homodimerization of gp130 in absence of ligand has also been previously described for two other gp130 mutants, Y190FV to AAA and Y190A[16]. Moreover, overexpression of wild-type gp130 impaired the activity of the mutant gp130 S187_Y190del in a dose-dependent manner (Fig 3e); therefore, mutant gp130 activity appears to be driven by its homodimerization that can be competed by the wild-type protein. Interestingly, using a reverse genetic approach in mice, Ernst and collaborators have recently shown that IL11 promotes chronic gastric inflammation and associated tumourigenesis mediated by gp130 and STAT3 activation[17]. In IHCA, we also found significant increases (6-fold) in the levels of *IL11* mRNA ($P<0.01$) that may serve to amplify gp130/IL6 signalling, despite a modest decrease in the expression of its specific receptor (*IL11RA*) (Supplementary Fig. S5a). However, in mutant gp130-expressing Hep3B cells *IL11* was not induced (Supplementary Fig. S5b), suggesting that elevation of *IL11* in IHCA in vivo may occur through secondary effects.

Relationships between activation of IL6 signalling and hepatic tumourigenesis have also been suggested from studies in mice, where transgenics that overexpress both IL6 and IL6R in hepatocytes develop large liver adenomas[18]. Further, in knock-in mice expressing gp130Y757 mutant, gastric inflammation and subsequent carcinoma development result from STAT3 activation[19-21]. The IL6 pathway is also known to activate SHP-2/RAS/ERK signalling[22]. While in humans STAT3 activation is a clear hallmark of gp130-mutated IHCA, phosphorylated ERK1/2 was only detected in 50% of these tumours (Supplementary Fig. S6a), and phospho-ERK1/2 was not

observed in Hep3B overexpressing mutant gp130 (Supplementary Fig. S6b). Thus, in contrast to STAT3 activation, activation of the SHP-2/RAS/ERK pathway does not appear to contribute to all IHCA.

Surprisingly, type 1 and type 2 interferon targets are overexpressed in gp130-mutated IHCA. Their aberrant activation here might be due to gp130-mediated STAT1/STAT2 activation and inefficient negative feedback by SOCS3, which is thought to prevent activation of type 2 interferon genes under physiological conditions[23]. Interestingly, the targets in gp130-mutated IHCA include *HIF1A* that encodes hypoxia-inducible factor-1ą which may contribute to VEGF overexpression and the "telangiectatic" phenotype of IHCA (Fig. 1b, 1c)[1,2,24]. Further, the inflammatory infiltrate that is a hallmark of IHCA may reflect the robust induction (~110-fold) of *CCL20* observed in all IHCA (Fig. 1b). Specifically, CCL20 is a chemokine that interacts with CCR6 and that directs chemoattraction of a wide spectrum of immune cells including dendritic cells and B and T lymphocytes[25], and such a scenario could direct or augment the inflammatory response seen in IHCA.

To investigate the possible interaction and cooperation of gp130 activation with other pathways altered in hepatocellular adenoma, we searched in the same series of 76 adenomas for *CTNNB1* (encoding β-catenin) and *HNF1A* mutations (encoding Hepatocyte Nuclear Factor 1α), two genetic alterations frequently associated with hepatocellular adenoma (HCA)[2,26,27]. HNF1α inactivation (22 cases) and gp130 activation (26 cases) were mutually exclusive in HCA ($P<10^{-4}$, Fisher exact test, Supplementary Table S4). By contrast, β-catenin activating mutations were found in 12 adenomas, and half of these had associated gp130 mutations. For two IHCA associated with a malignant transformation to carcinoma, both activating gp130 and β-catenin mutations were found (cases 469 and 786, Supplementary Table S4). In

one of these cases, we were able to genotype the hepatocellular carcinoma (HCC) and this harboured the same mutations in *CTNNB1* and *IL6ST* as the corresponding IHCA. In contrast, no cases of malignant transformation were observed in gp130-mutated IHCA without a β-catenin mutation (*P*=0.05, two-tailed Fisher exact test). When we sequenced *IL6ST* exon 6 in 111 HCC lacking a known history of IHCA[28], only two cases were mutated. Interestingly, these tumours were compatible with a malignant transformation of a non-diagnosed IHCA since both mutated HCC had inflammatory infiltrates; they harboured β-catenin-activating mutations and developed in non-cirrhotic liver (Supplementary Table S4). Collectively, these findings suggest cooperation between the IL6 and β-catenin pathways in the malignant transformation of IHCA.

IL6ST mutations were identified in 60% of IHCA. The remaining IHCA were, however, similar in their expression profiles as *IL6ST*-mutated IHCA (Supplementary Fig. S3) and, accordingly, activated nuclear phospho-STAT3 was also found in all non-mutated IHCA tested (Supplementary Fig. S4f). Sequencing of the functional domains of three gp130 co-receptors (*IL6R*, *LIFR,* and *OSMR*), the functional domains of three transducing proteins (*JAK2*, *JAK1*, and *TYK2*), and of the coding sequence of *SOCS3*, failed to identify mutations in gp130-non-mutated IHCA. Moreover, these tumours lacked mutations in the exons or intron/exon boundaries of *IL6ST*, and *IL6ST* mRNA levels were comparable to those expressed in normal hepatocytes (Supplementary Fig. S4a). Finally, no gain of chromosome 5q copy number at the *IL6ST* locus was observed using CGH-SNP experiments in gp130 mutated and non-mutated IHCA (data not shown). However, by western blotting and immunohistochemistry, we found that most IHCA cases overexpressed gp130 protein (Supplementary Fig. S4b-d), suggesting that the translation or turnover of gp130 is

affected in both gp130-non-mutated and mutated tumours. Therefore, gp130 overexpression and STAT3 activation are related to gp130 activating mutation in 60% of the IHCA, whereas in the non-mutated cases, the mechanism of STAT3 activation remains to be defined. Here, for example, activation may reflect mutations in a regulatory protein(s) that controls gp130 stabilisation, or be due to alterations in factors that control its translation.

The present findings reveal that STAT3 activation and the inflammatory phenotype in benign liver tumours can occur through gain-of-function somatic mutations in gp130. To our knowledge, this is the first identification of somatic mutation of gp130 in tumours and they define gp130 as an oncogene with involvement in benign human tumours. Our findings also underscore the important role of inflammatory response in hepatocellular tumourigenesis and are in accord with a recent study demonstrating that IL6 promotes liver tumour onset in mice[29]. Importantly, our studies also suggest that cooperating mutations of the WNT/β-catenin and IL6/STAT pathways in human liver tumours contribute to the occurrence of inflammatory hepatocellular carcinomas that develop in the absence of cirrhosis. More broadly, these findings indicate that this novel mechanism for activation of the IL6 signalling pathway should be interrogated in other human tumours, particularly those having an inflammatory phenotype and STAT3 activation, a hallmark of many epithelial tumours.

Methods summary

All tumours and corresponding non-tumour liver tissues were frozen after surgical resection. These tumours were clinically and genetically characterized; they were previously included in genetic and phenotypic studies (Supplementary Table S4 and refs. 1, 2 and 28). The study was approved by the local Ethics Committee (Paris Saint-Louis), and informed consent was obtained in accordance with French legislation. Transcriptional profiling were performed using Affymetrix oligonucleotide GeneChips HG-U133A and the microarray data have been deposited in Gene Expression Omnibus (GEO) under accession number GSE11819. Quantitative RT-PCR was performed as described[30] using pre-designed primers and probe sets from Applied Biosystems (provided in Supplementary Table S5). In all cases the somatic origin of the mutation found in tumour was verified by sequencing the corresponding adjacent, normal liver sample. In HEP3B cell experiments, all quantitative RT-PCR, luciferase assay and western blotting were performed two days after transfection and after 6 hours of serum starvation.

References

1. Bioulac-Sage, P. et al. Hepatocellular adenoma subtype classification using molecular markers and immunohistochemistry. *Hepatology* **46**, 740-8 (2007).
2. Zucman-Rossi, J. et al. Genotype-phenotype correlation in hepatocellular adenoma: new classification and relationship with HCC. *Hepatology* **43**, 515-24 (2006).
3. Grivennikov, S. & Karin, M. Autocrine IL-6 signaling: a key event in tumourigenesis? *Cancer Cell* **13**, 7-9 (2008).
4. Akira, S. et al. Molecular cloning of APRF, a novel IFN-stimulated gene factor 3 p91-related transcription factor involved in the gp130-mediated signaling pathway. *Cell* **77**, 63-71 (1994).
5. Wegenka, U.M., Buschmann, J., Lutticken, C., Heinrich, P.C. & Horn, F. Acute-phase response factor, a nuclear factor binding to acute-phase response elements, is rapidly activated by interleukin-6 at the posttranslational level. *Mol Cell Biol* **13**, 276-88 (1993).
6. Hibi, M. et al. Molecular cloning and expression of an IL-6 signal transducer, gp130. *Cell* **63**, 1149-57 (1990).
7. Boulanger, M.J., Chow, D.C., Brevnova, E.E. & Garcia, K.C. Hexameric structure and assembly of the interleukin-6/IL-6 alpha-receptor/gp130 complex. *Science* **300**, 2101-4 (2003).
8. Ward, L.D. et al. High affinity interleukin-6 receptor is a hexameric complex consisting of two molecules each of interleukin-6, interleukin-6 receptor, and gp-130. *J Biol Chem* **269**, 23286-9 (1994).
9. Lutticken, C. et al. Association of transcription factor APRF and protein kinase Jak1 with the interleukin-6 signal transducer gp130. *Science* **263**, 89-92 (1994).
10. Murakami, M. et al. IL-6-induced homodimerization of gp130 and associated activation of a tyrosine kinase. *Science* **260**, 1808-10 (1993).
11. Stahl, N. et al. Association and activation of Jak-Tyk kinases by CNTF-LIF-OSM-IL-6 beta receptor components. *Science* **263**, 92-5 (1994).
12. Coulouarn, C. et al. Genome-wide response of the human Hep3B hepatoma cell to proinflammatory cytokines, from transcription to translation. *Hepatology* **42**, 946-55 (2005).
13. Kishimoto, T., Akira, S., Narazaki, M. & Taga, T. Interleukin-6 family of cytokines and gp130. *Blood* **86**, 1243-54 (1995).
14. Chow, D., He, X., Snow, A.L., Rose-John, S. & Garcia, K.C. Structure of an extracellular gp130 cytokine receptor signaling complex. *Science* **291**, 2150-5 (2001).
15. Skiniotis, G., Boulanger, M.J., Garcia, K.C. & Walz, T. Signaling conformations of the tall cytokine receptor gp130 when in complex with IL-6 and IL-6 receptor. *Nat Struct Mol Biol* **12**, 545-51 (2005).
16. Li, H. & Nicholas, J. Identification of amino acid residues of gp130 signal transducer and gp80 alpha receptor subunit that are involved in ligand binding and signaling by human herpesvirus 8-encoded interleukin-6. *J Virol* **76**, 5627-36 (2002).
17. Ernst, M. et al. STAT3 and STAT1 mediate IL-11-dependent and inflammation-associated gastric tumourigenesis in gp130 receptor mutant mice. *J Clin Invest* **118**, 1727-38 (2008).
18. Maione, D. et al. Coexpression of IL-6 and soluble IL-6R causes nodular regenerative hyperplasia and adenomas of the liver. *Embo J* **17**, 5588-97 (1998).
19. Judd, L.M. et al. Gastric cancer development in mice lacking the SHP2 binding site on the IL-6 family co-receptor gp130. *Gastroenterology* **126**, 196-207 (2004).

20. Judd, L.M. et al. STAT3 activation regulates growth, inflammation, and vascularization in a mouse model of gastric tumourigenesis. *Gastroenterology* **131**, 1073-85 (2006).
21. Tebbutt, N.C. et al. Reciprocal regulation of gastrointestinal homeostasis by SHP2 and STAT-mediated trefoil gene activation in gp130 mutant mice. *Nat Med* **8**, 1089-97 (2002).
22. Boulton, T.G., Stahl, N. & Yancopoulos, G.D. Ciliary neurotrophic factor/leukemia inhibitory factor/interleukin 6/oncostatin M family of cytokines induces tyrosine phosphorylation of a common set of proteins overlapping those induced by other cytokines and growth factors. *J Biol Chem* **269**, 11648-55 (1994).
23. Croker, B.A. et al. SOCS3 negatively regulates IL-6 signaling in vivo. *Nat Immunol* **4**, 540-5 (2003).
24. Bioulac-Sage, P. et al. Clinical, morphologic, and molecular features defining so-called telangiectatic focal nodular hyperplasias of the liver. *Gastroenterology* **128**, 1211-8 (2005).
25. Schutyser, E., Struyf, S. & Van Damme, J. The CC chemokine CCL20 and its receptor CCR6. *Cytokine Growth Factor Rev* **14**, 409-26 (2003).
26. Bluteau, O. et al. Bi-allelic inactivation of TCF1 in hepatic adenomas. *Nat Genet* **32**, 312-5 (2002).
27. Chen, Y.W., Jeng, Y.M., Yeh, S.H. & Chen, P.J. P53 gene and Wnt signaling in benign neoplasms: beta-catenin mutations in hepatic adenoma but not in focal nodular hyperplasia. *Hepatology* **36**, 927-35 (2002).
28. Boyault, S. et al. Transcriptome classification of HCC is related to gene alterations and to new therapeutic targets. *Hepatology* **45**, 42-52 (2007).
29. Naugler, W.E. et al. Gender disparity in liver cancer due to sex differences in MyD88-dependent IL-6 production. *Science* **317**, 121-4 (2007).
30. Rebouissou, S. et al. HNF1alpha inactivation promotes lipogenesis in human hepatocellular adenoma independently of SREBP-1 and carbohydrate-response element-binding protein (ChREBP) activation. *J Biol Chem* **282**, 14437-46 (2007).

Acknowledgments: We are indebted to Philippe Bois (The Scripps Research Institute, Jupiter) and Olivier Bernard (Inserm E0210, Paris) for scientific discussion and critical reading of this manuscript. We warmly thank Cristel Thomas and Gaelle Cubel for their participation to this work that is dedicated to Jean-Philippe Salier (Inserm U519, Rouen). We also thank Jean Saric, Christophe Laurent, Antonio Sa Cunha, Brigitte Le Bail, Anne Rullier for contributing to the tissue collection (CHU Bordeaux). This work was supported by Inserm (Réseaux de recherche clinique et réseaux de recherche en santé des populations), the Ligue Nationale Contre le Cancer ("Cartes d'identité des tumeurs" program), ARC (grant 5158), and the

Fondation de France. S.R. and M.A. are supported by a fellowship from la Ligue Nationale Contre le Cancer and the Inca, respectively. JZR is supported by an interface contract between Inserm and Bordeaux hospital. TI is supported by the National Institutes of Health grants GM071596, AI055894, and AI067949.

Figures legends

Figure 1. Activation of the interleukin-6 and interferon pathways in inflammatory HCA. **a,** Immunohistochemical analysis of CRP expression: high level of expression in tumour hepatocytes (IHCA); adjacent normal non-tumour liver hepatocytes (NTL) and inflammatory cells located in tumour (arrow) are negative. **b,** qRT-PCR validation of gene array expression data comparing IHCA (n=14, black) to NTL (n=6, white). Graphs plot mean +/- SD. *, **, *** difference between groups at $P<0.05$; 0.01 and 0.001, respectively (two-tailed Mann-Whitney test). **c,** Western-blot analysis comparing expression levels of STAT1 (84, 91 kDa), STAT3 (79, 86 kDa), CRP (24 kDa), VEGF (22 kDa), Jak2 and phospho-Jak2 (125 kDa) between IHCA and NTL. **d,** Schematic representation of the IL6 and interferon pathways showing all genes overexpressed (red) or suppressed (green) in IHCA compared to NTL. Genes validated by qRT-PCR are underlined (IHCA n=14 versus NTL n=6); others were extracted from the microarray analysis (IHCA n=4 versus NTL n=4).

Figure 2. gp130 mutations in inflammatory hepatocellular tumours. **a,** The spectrum of mutations in gp130 detected in IHCA (S, signal peptide; TM, transmembrane domain). The location of the 16 deletions, the duplication (in blue), and the resulting amino acid substitutions (in yellow) identified in the D2 domain of gp130 are indicated above the wild type sequence (in bold font). The most frequent mutation is indicated in red. **b,** Residues 186-192 (shown in pink stick presentation) of the D2 domain of gp130 that are deleted in IHCA are intimately involved in interactions with IL6, as shown in the crystal structure of the IL6R:IL6:gp130 complex (PDB 1P9M)[7]. IHCA deletions 173-177 and 215 (labelled in red) are also predicted to disrupt the IL6-gp130 interface. The numbering of residues corresponds to the *IL6ST* cDNA, which has 22 additional *N*-terminal residues compared to the polypeptide chain due to the nuclear export signal.

Figure 3. Gain-of-function mutations of gp130. a, Gp130 mutants (Δ) including S187_Y190del (S), Y186_Y190del (Y), V184_Y186del, S187A (V) and K173_D177del (K) or

controls including gp130 wild type (Wt) and empty plasmid (EP) were transfected in Hep3B. Graphs plot qRT-PCR results relative to EP transfected unstimulated cells, mean +/- SD (transfections in triplicate). **b**, Graph plots luciferase activity (mean) measured in triplicate transfections (+/-SD) with pSTAT3-luc alone or together with Wt or the ΔS gp130. Expression of total and phosphorylated (p-STAT3 and p-gp130) proteins were analysed using western blotting, after immunoprecipitation (IP) for gp130. **c**, *CRP* mRNA expression after transfection with increasing amounts of plasmids expressing Wt or ΔS gp130 (baseline, mock-transfected cells). **d**, Hep3B transfected with EP, Wt or ΔS gp130 and exposed to increasing concentrations of IL6. Graph plots mean *CRP* expression value relative to cells transfected with EP +/- SD (transfections in triplicate). **e**, Effect of increasing amounts of Wt gp130 on the ΔS gp130 mutant activity, without IL6. Graph plots mean level of expression of SOCS3 and CRP relative to cells transfected with EP +/- SD in duplicate (left) or in 5 independent transfections (right). **f,** Flag and Myc-tagged constructs expressing either the wild-type or the mutant ΔS gp130 were co-transfected (1:1) into Hep3B. gp130 dimers formation was detected after immunoprecipitation using the anti-flag antibody, followed by western blot analysis with the anti-myc and anti-flag antibodies. Shown is one representative of three independent experiments. *, **, *** indicate differences between groups at $P<0.05$; 0.01 and 0.001, respectively (two-tailed t-test).

Supplementary Figures

Supplementary Figure S1. Immunohistochemical analysis of the inflammatory response in IHCA. This IHCA overexpressed SAA (**a**) and CRP (**b**) with a sharp demarcation from the non-tumoural liver (NTL). Only hepatocytes of the IHCA expressed SAA or CRP; inflammatory infiltrates are negative for these acute phase inflammation proteins (asterix). Inflammatory infiltrates are made predominantly of lymphocytes ($CD45^+$), localized around vascular axis inside the tumour (c); T lymphocytes ($CD3^+$) with CD4/CD8 (d-f) ratio around 2/1 are more numerous than B lymphocytes ($CD20^+$) (g), intermingled with $CD68^+$ histiocytes (h).

Supplementary Figure S2. Example of somatic DNA alterations identified in exon 6 of the *IL6ST* gene. Boundaries of the deletions are indicated by an arrow; mutated sequences are represented below the *IL6ST* wild-type sequence. **a,** Forward sequence of one representative case of mutated IHCA (T) and its matching non-tumour DNA (N) showing the somatic origin of the most frequent deletion identified; the nucleotide sequence deleted in tumour 382 is boxed. Amino acids (AA) and nucleotides (NT) are numbered according to *IL6ST* cDNA ORF. **b,** cDNA sequence analysis of two cases of mutated IHCA (T), showing expression of both the wild type and the mutant allele. **c**, Individual 770 is heterozygous for the polymorphism rs3729960 (697 G>C leading to G148R) located in exon 5 (arrow). The same ratio of allele is observed in normal and tumour sample both at the DNA and cDNA level. As this polymorphism is amplified in the same cDNA fragment than the mutated exon 6, these results show that the wild-type and the mutated allele are expressed at the same level in IHCA.

Supplementary Figure S3. Comparison of expression profiles between gp130 mutated inflammatory HCA and gp130 non-mutated IHCA. Comparison was carried out for the 24 genes validated by quantitative RT-PCR that were significantly differentially expressed between IHCA and non-tumour livers. Seven gp130 mutated IHCA (in black) were compared to 7 gp130 non-mutated IHCA (in grey). Results are expressed as mean ± SD; * difference between groups at $P<0.05$ (two-tailed Mann-Whitney test).

Supplementary Figure S4. Analysis of gp130 and p-STAT3 expression in inflammatory HCA. **a,** *IL6ST* mRNA level in 6 non-tumour livers (NTL) was compared with that of 7 gp130-mutated IHCA (M) and 7 gp130-non-mutated IHCA (NM), using qRT-PCR. Results are expressed as mean-fold difference ± SD, relative to NTL; ns: non significant (two-tailed Mann-Whitney test). **b,** Western-blotting analysis of gp130 protein level in 3 non-tumour livers (NTL), 2 gp130-mutated IHCA and 7 gp130-non-mutated IHCA. Red ponceau staining was used as loading control. **c**, **d**, Immunohistochemical analysis of gp130 showing

overexpression of the protein in both gp130-mutated (**c**) and gp130-non-mutated (**d**) IHCA compared to their adjacent non-tumour liver parenchyma (NTL). **e**, **f**, **g**, Immunohistochemistry of phospho-STAT3 (tyr705) in gp130-mutated (**e**) and non-mutated (**f**) IHCA showing an intense nuclear staining in tumour cells while p-STAT3 is undetectable in non-tumour liver (NTL) (**g**).

Supplementary Figure S5. **mRNA expression of *IL11* and *IL11RA* in inflammatory HCA and transfected Hep3B cells. a**, *IL11* and *IL11RA* mRNA levels were assessed using qRT-PCR in 6 non-tumour livers (NTL), 7 gp130-mutated IHCA (M) and 7 gp130-non-mutated IHCA (NM). Results are expressed as mean-fold difference ± SD, relative to NTL (mean NTL=1) *, **, difference between groups at $P<0.05$ and 0.01, respectively (two-tailed Mann-Whitney test). **b**, qRT-PCR analysis of *IL11* mRNA expression in Hep3B cells transfected either with Wt gp130 or with four IHCA mutants of gp130 (Δ) (Y186_Y190del (Y); K173_D177del (K); S187_Y190del (S) and V184_Y186del, S187A (V)), as described in Fig3. Experiments were performed in triplicate and expressed as mean ± SD in comparison to empty plasmid-transfected and untreated cells (mean=1). ns: non significant (two-tailed t-test).

Supplementary Figure S6. Western blotting analysis of ERK1/2 activation in inflammatory HCA and Hep3B cells. **a**, Expression of the phosphorylated forms of ERK1 and ERK2 was compared between 10 IHCA (including 4 cases mutated for gp130) and 6 non-tumour livers (NTL). Red ponceau staining was used as loading control. **b**, Expression of phospho-ERK1/2 was compared between Hep3B cells transfected with the wild-type (Wt) or the mutant (ΔS) gp130 (S187_Y190del). As a control cells were transfected with empty plasmid and untreated or stimulated with 100 ng/µl of IL6.

Methods

A series of 76 HCA was analysed. All samples were collected in Bordeaux hospital. They were extensively characterised and included in previous studies[1,2]. All the 111 HCC were included and described previously[28]. For each tumour, a corresponding frozen non-tumour liver sample was available for analyses.

Transcriptome analyses

Transcriptional profiling of four IHCA and four normal liver tissues were performed using Affymetrix oligonucleotide GeneChips HG-U133A (GEO accession number GSE11819). For each case, 5 µg of total RNA were labeled and hybridization was performed using 20 µg of cRNA per hybridization (GeneChip Fluidics Station 400), according to the manufacturer's instructions (Affymetrix, Santa Clara, CA). Array images were digitized by using Microarray Suite 5.0 (MAS5) software, embedded in the Affymetrix GeneChip Operating Software (Affymetrix, Santa Clara, USA). Gene intensity derivation was carried out from the raw numerical data (CEL files) by using the R package affy[31], available as part of the Bioconductor project[32], and the DNA-Chip analyzer (dChip) program[33]. Probe sets corresponding to control genes or having a "_x_" annotation were masked yielding a total of 19,787 probe sets available for further analyses. Background subtraction, normalization and expression summaries for every probe set were calculated with the log-scale robust multi-array analysis (RMA) algorithm using a background adjusted PM intensities model[34], and with the model-based expression indexes (MBEI) calculation following a PM/MM difference model[33]. The log-transformed normalized data was considered for further analysis; and a gene annotation was adjoined using the Unigene cluster identifier as a common primary key (Unigene Build184-June05).

Differential analyses were performed using multiple testing procedures to evaluate statistical significance for differentially expressed genes. The biological groups were compared as independent conditions. A pooled curve-fit error method was used for random error estimation; a range of 3.0 median absolute deviations (MADs) to 4.0 MAD established outlier-detection thresholds automatically. Data were subjected to iterative normalization by centering to the median across biological groups. Statistical analyses were computed using both z- and t-statistics including a p-value ranking. Considering respective tests, a false discovery rate (FDR) adjustment of the p-values was used for multiple testing corrections, and permutation tests (n>1000) were computed to control the proportion of false discoveries (i.e. false positives, > 90% confidence). Only genes whose expression significantly differed between inflammatory HCA versus non-tumour liver tissues (considering absolute fold change > 1.5 and p-values ≤ 0.01) were selected.

Gene ontology (GO) categories that were significantly over-represented in genes significantly up-regulated or suppressed in inflammatory HCA were determined by the hypergeometric test using the web-based tool GOTree Machine (GOTM) (http://bioinfo.vanderbilt.edu/gotm/) by comparison with the distribution of the overall genes included in the HG-U133A Affymetrix array.

Quantitative RT-PCR

Quantitative RT-PCR was performed in duplicate as described[30]. Ribosomal 18S RNA (*R18S*) was used to normalize expression data and $2^{-\Delta\Delta CT}$ method was applied. Final results were expressed as the n-fold differences in target gene expression in tested samples when compared with the mean expression value of non-tumour tissues (for tumour analysis) or with control cell line.

DNA sequencing

DNA sequencing was performed as described[26] using primers provided in Supplementary Table S6. All mutations were validated by sequencing a second independent PCR product on both strands.

Cell culture

Hep3B cells (ATCC) were grown in DMEM supplemented with 10% fetal calf serum. For transfections, cells were plated 16h prior to transfection to produce monolayers that were 60% confluent and these were transfected by using Lipofectamine™ LTX according to the manufacturer's instructions (Invitrogen). Transfection efficiency was monitored by measuring the level of either wild-type and mutated gp130 mRNA using quantitative RT-PCR and western blot analysis. The same gp130 expression level was observed in wild-type and mutant transfected cells. 48h after transfection, cells were maintained in serum-free medium, then cells were either left untreated or were stimulated with rhIL-6 (100 ng/ml) in a serum-free medium for 3 hr, just before cell harvest and protein and RNA extraction. For luciferase assay, Hep3B cells were co-transfected with Stat3 luciferase reporter vector (pSTAT3-luc 0.5µg, Panomics) and the expression plasmid for wild type or S187_Y190del mutant (ΔS) gp130 (1µg). Two days after transfection, the cells were lysed and the luciferase activity was measured according to the manufacturer's recommendations (Promega). The activities were normalized to protein in each cell lysate.

Generation of gp130 mutants

A full-length gp130 open reading frame cloned in pORF9 vector was purchased from Invivogen (pORF9-hIL6ST). Mutagenesis reactions were performed using the QuickChange site-directed mutgenesis kit (Stratagen). All constructs were verified by

sequencing. Using the same method, we also introduced two different epitope tags (myc and flag) at the C-terminal end in the wild-type and S187_Y190del constructs.

Western blot analysis and immunoprecipitation

Western blot analyses were performed as described[30] using the antibodies specific for STAT3, phospho-STAT3 Tyr705, STAT1, phospho-JAK2 Tyr1007/1008 (Cell Signaling Technology, diluted 1:500), JAK2 (Santa Cruz Biotechnology, 1:500), CRP (Sigma, 1:500), gp130 (C-20 Santa Cruz Biotechnology, 1:200), and VEGF (Novus Biologicals, 1:100). The phosphorylated form of gp130 (p-gp130) was analysed by SDS-PAGE after immunoprecipitation from cell lysates containing 750 µg of proteins using 5µg of the C-20 anti-gp130 antibody. The membrane was then probed with antibodies directed against phosphotyrosine (clone 4G10, Upstate Biotechnology) and gp130 (C20). For dimerization assays, cell lysates were incubated with Protein G agarose (Pierce) and anti-flag antibody (Cell signaling technology, 1:50), at 4°C overnight. The immune complexes were sedimented, washed, separated by SDS-PAGE and analysed by Western blot using anti-flag (1:1000) and anti-myc (1:1000) antibodies. In western blot, red ponceau staining or actin (Sigma, 1:3000) expression was analysed to appreciate protein loading.

Immunohistochemistry

Immunohistochemistry was performed using a Dako autostainer, on paraffin sections of 10% fixed tumour tissue using 2 monoclonal antibodies against inflammatory proteins: anti-C-reactive protein (CRP), (Abcam, 1:1500), anti-serum amyloid A (SAA), (Dako, 1:50), anti-phospho-STAT3 Tyr705 (Cell signaling Technology, 1:50), anti-gp130 (C-20 Santa Cruz Biotechnology, 1:200). For

inflammatory cells immunotyping, the following antibodies (Dako) were used: CD45 (clone EB11+PD7/26, 1:300), CD3 (polyclonal, 1:100), CD4 (clone OPD4, 1:100), CD8 (clone C8/144B, 1:20), CD20 (clone L26, 1:100), CD68 (clone PG-M1, 1:50). For each immunohistochemical procedure, antigen retrieval was performed in citrate buffer, detection was amplified by the Dako Envision system.

Methods additional references

31. Gautier, L., Cope, L., Bolstad, B.M. & Irizarry, R.A. Affy--analysis of Affymetrix GeneChip data at the probe level. *Bioinformatics* **20**, 307-15 (2004).
32. Gentleman, R.C. et al. Bioconductor: open software development for computational biology and bioinformatics. *Genome Biol* **5**, R80 (2004).
33. Li, C. & Hung Wong, W. Model-based analysis of oligonucleotide arrays: model validation, design issues and standard error application. *Genome Biol* **2**, Research0032 (2001).
34. Irizarry, R.A. et al. Summaries of Affymetrix GeneChip probe level data. *Nucleic Acids Res* **31**, e15 (2003).

Table 1. gp130 somatic mutations identified in inflammatory hepatocellular tumours

Number of mutated tumours	Nucleotide change*	Amino acid change*
6**	560_571del	S187_Y190del
4**	557_571del	Y186_Y190del
3	565_576del	V189_V192del
2	563_574del	T188_F191del, V192I
1	503_580del	K168_N192del
1**	518_532del	K173_D177del
1**	551_559del	V184_Y186del, S187A
1	557_574del	Y186_F191del, V192F
1	559_573del	S187_F191del
1	564_575del	T188_F191del, V192T
1	569_577del, 578A>C	Y190_V192del, N193S
1	573T>G, 574_582del	F191L, V192_I194del
1	575_583del	V192_I194del
1	577_579del, 580A>T	N193del, I194F
1	583_588del	E195_V196del
1	614_646dup	K206_P216dup, G205R
1	643_645del	D215del

*Codons and mutated nucleotides are numbered according to IL6ST cDNA ORF

**gp130 mutants analysed in Hep3B cells

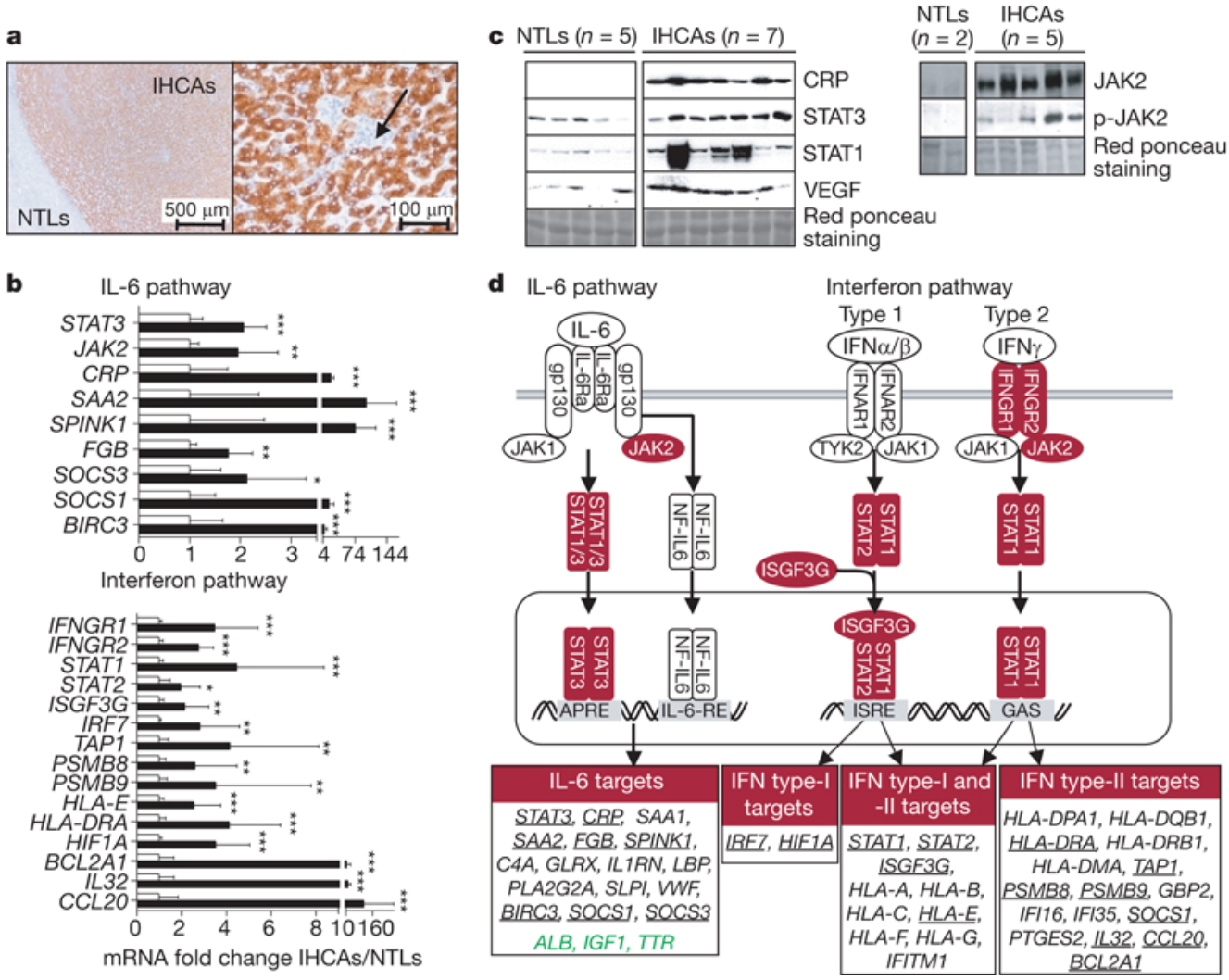
a
IHCAs
NTLs
500 μm
100 μm
b
IL-6 pathway
STAT3
JAK2
CRP
SAA2
SPINK1
FGB
SOCS3
SOCS1
BIRC3
0 1 2 3 4 74 144
Interferon pathway
IFNGR1
IFNGR2
STAT1
STAT2
ISGF3G
IRF7
TAP1
PSMB8
PSMB9
HLA-E
HLA-DRA
HIF1A
BCL2A1
IL32
CCL20
0 2 4 6 8 10 160
mRNA fold change IHCAs/NTLs
c
NTLs (n = 5)
IHCAs (n = 7)
CRP
STAT3
STAT1
VEGF
Red ponceau staining
NTLs (n = 2)
IHCAs (n = 5)
JAK2
p-JAK2
Red ponceau staining
d
IL-6 pathway
Interferon pathway
Type 1
Type 2
IL-6
gp130
IL-6Ra
IFNα/β
IFNAR1
IFNAR2
IFNγ
IFNGR1
IFNGR2
JAK1
JAK2
TYK2
STAT1/3
NF-IL6
STAT1
ISGF3G
STAT3
APRE
IL-6-RE
ISRE
GAS
IL-6 targets
STAT3, CRP, SAA1, SAA2, FGB, SPINK1, C4A, GLRX, IL1RN, LBP, PLA2G2A, SLPI, VWF, BIRC3, SOCS1, SOCS3
ALB, IGF1, TTR
IFN type-I targets
IRF7, HIF1A
IFN type-I and -II targets
STAT1, STAT2, ISGF3G, HLA-A, HLA-B, HLA-C, HLA-E, HLA-F, HLA-G, IFITM1
IFN type-II targets
HLA-DPA1, HLA-DQB1, HLA-DRA, HLA-DRB1, HLA-DMA, TAP1, PSMB8, PSMB9, GBP2, IFI16, IFI35, SOCS1, PTGES2, IL32, CCL20, BCL2A1

QuickTime™ et un
décompresseur
sont requis pour visionner cette image.

Figure 1

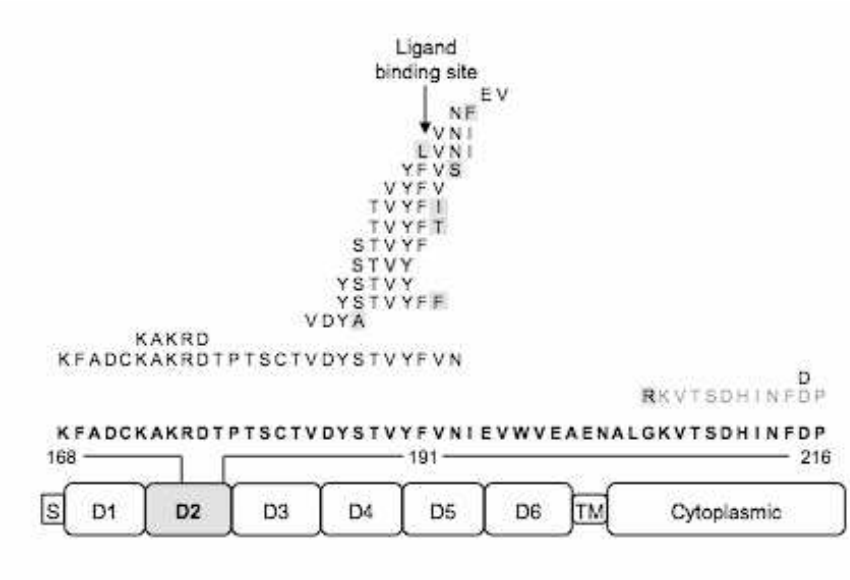

Figure 2a

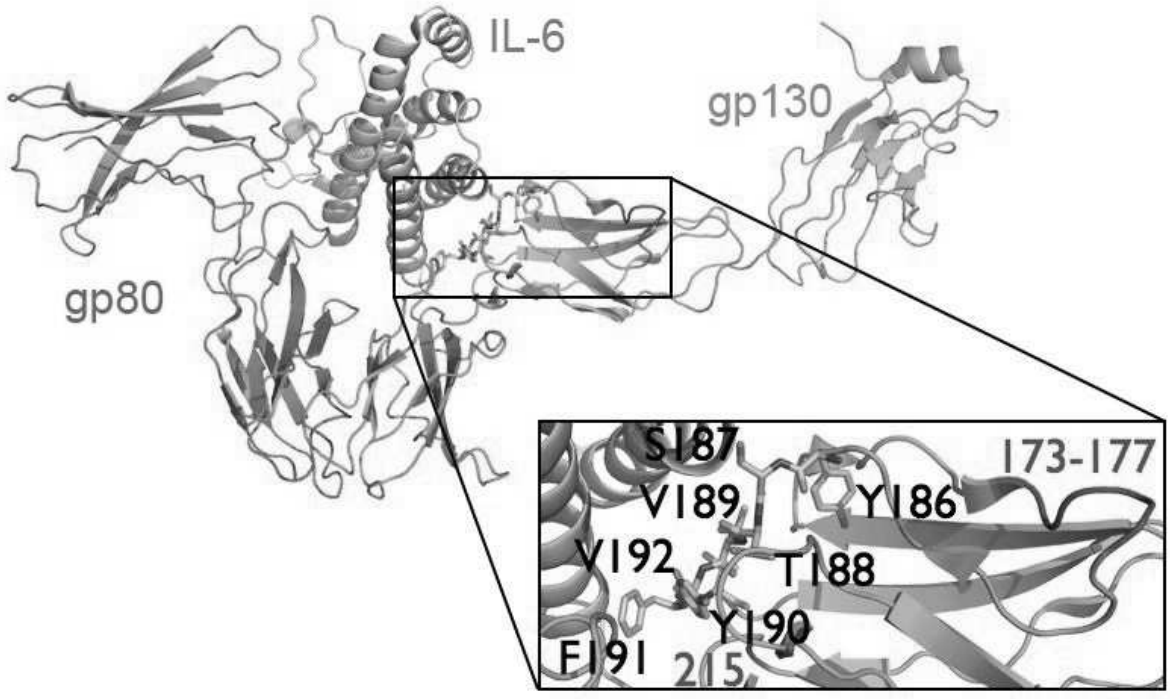

Figure 2b

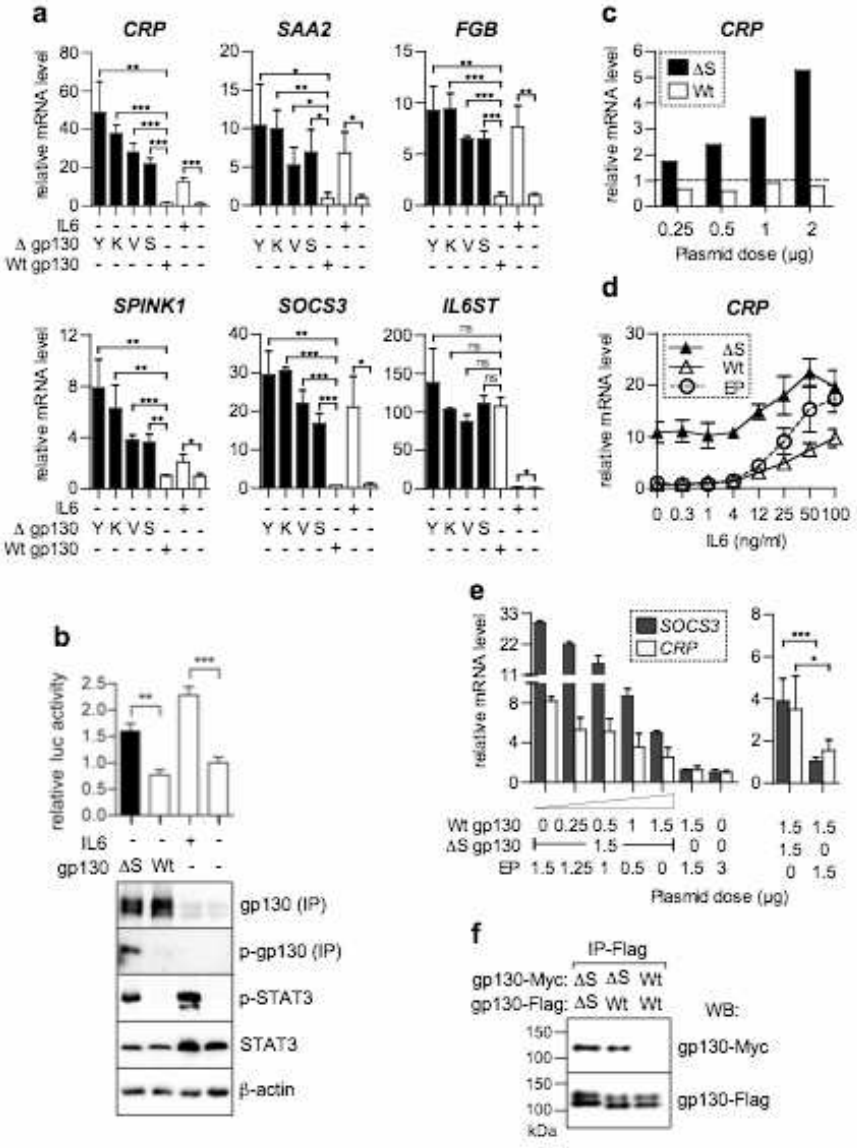
a
CRP
SAA2
FGB
SPINK1
SOCS3
IL6ST
relative mRNA level
IL6
Δ gp130 Y K V S
Wt gp130
b
relative luc activity
gp130 ΔS Wt
gp130 (IP)
p-gp130 (IP)
p-STAT3
STAT3
β-actin
c
CRP
ΔS
Wt
Plasmid dose (μg)
d
CRP
ΔS
Wt
EP
IL6 (ng/ml)
e
SOCS3
CRP
Wt gp130
ΔS gp130
EP
Plasmid dose (μg)
f
IP-Flag
gp130-Myc: ΔS ΔS Wt
gp130-Flag: ΔS Wt Wt
WB:
gp130-Myc
gp130-Flag
kDa

Figure 3